

***Ab initio* studies of Cs on GaAs (100) and (110) surfaces**

Siddharth Karkare* and Laurent Boulet

CLASSE, Cornell University, Ithaca, New York, USA

Arunima Singh

Department of Materials Science and Engineering, Cornell University, Ithaca, New York, USA

Richard Hennig

*Department of Materials Science and Engineering, Cornell University, Ithaca, New York, USA
and Department of Materials Science and Engineering, University of Florida, Gainesville, Florida, USA*

Ivan Bazarov

CLASSE, Cornell University, Ithaca, New York, USA

(Received 24 October 2014; published 12 January 2015)

GaAs with an atomic monolayer of Cs is one of the best known photoemissive materials. The results of density functional theory calculations of Cs adsorption on the GaAs(100)-(4 × 2) gallium-terminated reconstructed surface and the GaAs(110) surface are presented in this work. Coverage of up to 4 Cs atoms/nm² on GaAs surfaces has been studied to predict the work-function reduction and adsorption energies accurately. The high mobility of Cs atoms on the (110) surface allows formation of ordered structures, whereas the low mobility of Cs of the (100) surface causes amorphous growth.

DOI: [10.1103/PhysRevB.91.035408](https://doi.org/10.1103/PhysRevB.91.035408)

PACS number(s): 68.43.Bc

I. INTRODUCTION

GaAs activated using Cs is an excellent photoemitter and has found numerous applications as a source of both spin-polarized [1] and nonpolarized electrons in photoinjectors [2] and as an infrared light sensor in image intensifiers [3]. An ideal photoemitter should have a high quantum efficiency (QE), low mean transverse energy (MTE) of the emitted electrons, a short response time, good lifetime, and low sensitivity to nonideal vacuum conditions. Despite its very stringent requirements on vacuum, GaAs activated using Cs remains an excellent photoemitter due to its high QE in visible and near-infrared light and the low MTE of emitted electrons [4].

The process of photoemission from activated GaAs has been best explained using Monte Carlo electron transport simulations within the framework of Spicer's three-step photoemission model [5]. This model divides the process of photoemission into three steps: (i) the excitation of electrons by photon absorption, (ii) the transport of excited electrons to the surface, and (iii) the emission of electrons reaching the surface into vacuum. While the steps of excitation and transport are well understood, the emission of electrons into vacuum uses several *ad hoc* assumptions to explain experimental results [5].

Assuming conservation of transverse momentum at the surface due to translational invariance and the small electron effective mass in the Γ valley of the first conduction band in GaAs, the emitted electrons should exhibit very low MTE of less than 5 meV [5,6]. However, even for the best quality GaAs(100) surfaces grown using molecular beam epitaxy, experimental observations indicate MTE values of 25–100 meV [7]. The larger MTE values have been explained

by introducing an *ad hoc* scattering at the surface due to the nonconservation of transverse momentum. The cause of this scattering has not been understood. Understanding the structure of the Cs layer is important to identify the surface scattering mechanism responsible for the increased MTE.

Photoemission from GaAs can be obtained by depositing only 0.5–1 monolayer (ML) of Cs on the surface. Different authors define a monolayer of Cs differently, and hence to avoid confusion we do not use the monolayer notation and instead use the surface density of Cs atoms/nm², with the typical 1 ML thought to roughly correspond to 4–8 Cs atoms/nm².

The adsorption of Cs on GaAs has been studied for decades. Numerous surface studies of Cs on the (100) and (110) surfaces of GaAs have been performed using Auger spectroscopy, low-energy electron diffraction (LEED), and scanning tunneling microscopy (STM). The two surfaces show very different Cs adsorption characteristics. Cs adsorbs on the (110) surface to form one-dimensional (1D) structures at low coverages. At higher coverages greater than 2.2 Cs atoms/nm² the lines form two-dimensional (2D) polygons which merge to form a (4 × 4) structure. This structure has been observed by LEED [8,9] and STM [10,11]. Formation of such structures is evidence that the Cs atoms are mobile on the GaAs(110) surface. On the other hand, both LEED and STM studies confirm the formation of an amorphous layer [12–14] on the (100) surface and no ordered 1D or 2D structures of Cs atoms are observed. Various experimental studies have characterized the Cs activation of the (100) and (110) surfaces by measuring the photoemission current, work-function reduction, strength of the Auger Cs signal, and Cs adsorption energies as a function of Cs dosage [8,9,12–19]. However, a complete theoretical understanding of these characteristics and differences is still lacking.

Density functional theory (DFT) has proven helpful in the study of the work function of various materials [20–24]. DFT

*ssk226@cornell.edu

correctly predicts that the adsorption of Cs on transition metal surfaces lowers the work function through the formation of a surface dipole [21]. DFT calculations for isolated Cs atoms adsorbed on As- and Ga-terminated GaAs(100) surfaces have shown that Cs is preferentially located surrounded by As [23,24]. However, only low Cs coverages (<1 atom/nm²) and not all possible adsorption sites were considered.

In this paper, we report DFT calculations for Cs adsorbed on the Ga-terminated (100) and the (110) surfaces of GaAs for Cs surface densities of up to 4 atoms/nm². For low Cs surface densities (<1 atom/nm²), we compute the diffusion activation energy for Cs atoms to move on the GaAs surface, allowing us to compare the mobility of Cs atoms on the (110) and the (100) surfaces. The low mobility on the (100) surface can explain the formation of the amorphous Cs layer, while the higher mobility on the (110) surface is consistent with the experimentally observed formation of the ordered (4×4) epitaxial layer. For higher Cs coverages, we show that the preferred adsorption sites of the Cs atoms change with the surface density of Cs atoms and find that the resulting work-function reduction and the adsorption energies agree well with experimental data. Our study of Cs adsorption on GaAs surfaces demonstrates the feasibility of using computational approaches to discover new photoemissive surfaces and structures.

II. SIMULATION METHODS AND DETAILS

A. Computational methods

All calculations are performed using the plane-wave DFT code VASP, which utilizes the projector-augmented wave (PAW) method [25–27]. Throughout this work, the generalized gradient approximation (GGA) with the Perdew-Burke-Ernzerhof (PBE) parametrization is used [28]. The PAW potentials described for Ga and As assume a [Ar] core and for Cs a [Kr] $4d^{10}$ core, resulting in 3, 5, and 9 valence electrons, respectively. A plane-wave cutoff energy of 400 eV and a $4 \times 4 \times 1$ k -point mesh ensure a convergence of the energy to 2 meV/atom. The structures are relaxed until the forces are below 0.01 eV/Å.

B. Surface structures

The calculations for both the gallium-terminated GaAs(100)-(4×2) surface and the GaAs(110) surface were performed using a slab geometry with a vacuum layer of 25 Å, which was found to be sufficient to make interactions between the slabs negligible. The number of atomic layers in both slabs was chosen sufficiently large to converge the surface energy to 1.3 meV/Å². The work function for each surface is determined by the difference between the highest occupied band of the surface slab and the electrostatic potential in the vacuum. The vacuum potential is taken as the average electrostatic potential halfway between the periodic slabs. To accurately describe the electrostatic potential in the vacuum region, a dipole correction is added along the direction perpendicular to the slabs.

Figures 1(a) and 1(b) show the slab for the GaAs(100)-(4×2) surface consisting of nineteen atomic layers and containing 140 atoms. The size of the cell was $7.995 \text{ \AA} \times 15.990 \text{ \AA} \times 50.440 \text{ \AA}$. The (4×2) surface reconstruction of the Ga-terminated (100) surface exhibits a dimer reconstruction [23].

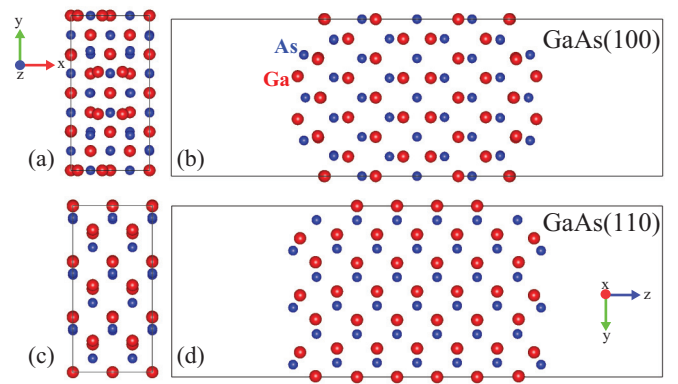


FIG. 1. (Color online) (a) Top and (b) side view of the relaxed Ga-terminated GaAs(100)-(4×2) surface slab. (c) Top and (d) side view of the relaxed GaAs(110) surface. Both cells have a vacuum spacing of 25 Å, which sufficiently reduces interactions between the slabs. The Ga atoms are shown in red and the As atoms are shown in blue. For the (100) surface the x , y , and z axes indicate the [011], $[0\bar{1}1]$, and [100] directions, respectively. For the (110) surface the x , y , and z axes indicate the $[00\bar{1}]$, $[\bar{1}10]$, and [110] directions, respectively.

After relaxation our calculations reproduced the previously computed structural parameters to an accuracy of 1% [23]. It is important to note that in this work we use the GaAs reconstruction on both sides of the slab and do not use hydrogen termination on one side, as done in previous works [23,29]. During relaxation, atoms in the four outermost layers were allowed to move and the remaining atoms were kept fixed.

Figures 1(c) and 1(d) illustrate the computational cell for the GaAs(110) slab consisting of 11 atomic layers and containing 156 atoms. The size of the cell was $7.995 \text{ \AA} \times 16.961 \text{ \AA} \times 48.986 \text{ \AA}$. The GaAs(110) surface is stable and does not show any reconstruction. Nevertheless, the surface As atoms relax outwards, to a position slightly above the surface Ga atoms [30]. Our DFT calculations reproduce the same behavior. During relaxation the atoms in the two outermost layers were allowed to move and the remaining atoms were fixed to the bulk position.

To estimate the mobility of Cs atoms on GaAs surface, we calculate the energy barrier for surface diffusion. The energy barriers for pathways connecting the lowest-energy adsorption sites are calculated using the nudged elastic band method [31,32], allowing the atomic positions of the top two layers of the slab to relax.

C. Cs adsorption calculations

We study several configurations for five different surface densities of Cs atoms, corresponding to 1–5 Cs atoms on the simulation cell surface. Cs atoms are placed at random x and y positions and at a z position 3.2 Å away from the outermost surface atom with a minimum allowed Cs-Cs distance of 4.0 Å. The Cs atoms along with the outermost four layers for the (100) surface and two layers for the (110) surface of the GaAs slabs were allowed to relax. This is repeated several times for each density of Cs atoms to obtain a statistical sampling.

To reduce the computational cost of generating the relaxed configurations, different Cs configurations are placed on the top and bottom surface of the slabs, doubling the number of relaxed configurations. The number of relaxed configurations, n , is 20 for 1–5 Cs atoms on the (110) surface. For the (100) surface, the number of configurations is 20 for one to three Cs atoms, 18 for the four-Cs-atoms case, and 12 for five Cs atoms.

The energy for each relaxed Cs configuration is obtained by separate calculations where Cs atoms are only adsorbed on one surface. The total adsorption energy of N number of Cs atoms per surface per simulation cell is given by $\Delta E_N = (E_{\text{slab}} + NE_{\text{Cs}}) - E_{\text{slab}+\text{Cs}}$, where E_{slab} is the energy of the relaxed GaAs slab without any Cs atoms, E_{Cs} is the energy of a free Cs atom in vacuum, N is the number of adsorbed Cs atoms, and $E_{\text{slab}+\text{Cs}}$ is the energy of the slab with the relaxed Cs atoms on one surface.

Thermodynamic averages at room temperature for observables Q_N , as a function of the number of Cs atoms, such as the adsorption energy, Cs atom position distribution, or work function, are estimated assuming classical thermodynamics using

$$\langle Q_N \rangle = \frac{\sum_{i=1}^n Q_N^i \exp\left(-\frac{\Delta E_N^i}{k_B T}\right)}{\sum_{i=1}^n \exp\left(-\frac{\Delta E_N^i}{k_B T}\right)}, \quad (1)$$

where k_B is the Boltzmann constant, $T = 293$ K corresponds to room temperature, and the superscript i denotes the i th configuration. The thermodynamically weighted standard deviation σ_Q is given by

$$\sigma_{Q_N} = \sqrt{\langle (Q_N - \langle Q_N \rangle)^2 \rangle}. \quad (2)$$

The chemical potential of Cs is defined as the energy released by adding a Cs atom to the surface and is estimated from the average adsorption energies by $\mu_{\text{Cs}} = \langle \Delta E_N \rangle - \langle \Delta E_{N-1} \rangle$. The work function is defined as the energy difference $\langle W \rangle = \langle E_{\text{vac}} - E_{\text{fermi}} \rangle$ between the energy of the electrostatic potential in the vacuum region E_{vac} and the energy of the highest occupied orbital in the slab E_{fermi} [20–22].

The position distribution of Cs atoms on the surface is calculated using a Gaussian smearing. For the purpose of visualization in Fig. 3, the (x, y) coordinates of the Cs atoms are convolved with a truncated 2D Gaussian function of width $\sigma = 1.75 \text{ \AA}$ ($1/\sqrt{2}$ times the covalent bonding radius of Cs) and a truncation radius equal to σ . The position distributions are averaged following Eq. (1).

III. RESULTS AND DISCUSSION

A. Mobility of Cs at low coverages

Figure 2 shows the low-energy equilibrium positions of a single Cs atom on the (110) and (100) surfaces of GaAs and the minimum-energy path for Cs diffusing between the equilibrium positions. For the (100) surface the most stable position, labeled as I , has an adsorption energy of 2.55 eV and lies in a trench away from the dimer reconstruction. Figures 2(a) and 2(b) illustrate the minimum-energy paths for diffusion along the trench ([011] direction) and to cross over the dimer reconstruction ([01 $\bar{1}$] direction) on GaAs(100),

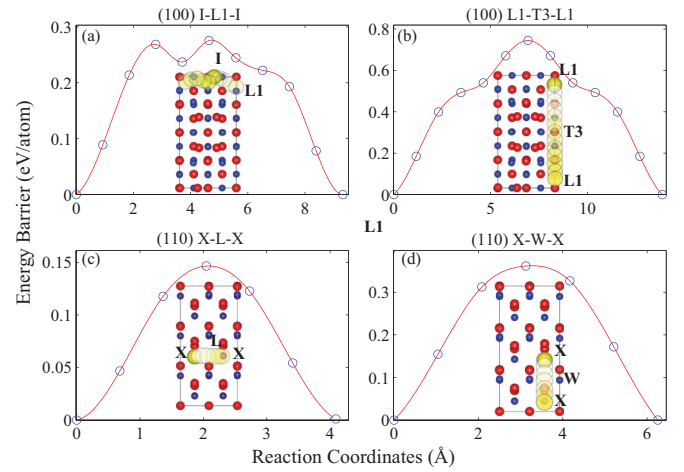


FIG. 2. (Color online) The energy barrier for the diffusion of Cs, (a) along the trench ([011] direction) on GaAs(100), (b) across the dimer ([01 $\bar{1}$] direction) on GaAs(100), (c) between two adjacent X sites along the [00 $\bar{1}$] direction on GaAs(110), and (d) between two adjacent X sites along the perpendicular [1 $\bar{1}$ 0] direction on GaAs(110). Ga atoms are shown in red and As atoms in blue. The initial position of the diffusing Cs atom is shown as a yellow sphere, and subsequent images along the minimum-energy path of the Cs atom are shown as circles, with the darkest circle denoting the final position.

proceeding through a metastable minimum, labeled $L1$. In order to move along the trench (in the [011] direction), the Cs atom follows the path $I - L1 - I$ with a low-energy barrier of only 0.28 eV. The crossing over the dimer reconstruction proceeds through the saddle point labeled $T3$ with a resulting energy barrier of $E_{T3} - E_I = 0.96$ eV.

For the (110) surface the most stable position, labeled as X , has an adsorption energy of 1.71 eV. Figures 2(c) and 2(d) illustrate the minimum-energy paths between neighboring X positions. The energy barrier for the Cs atom to move along the [00 $\bar{1}$] direction is 0.15 eV, while the barrier to move in the perpendicular direction ([1 $\bar{1}$ 0]) is 0.35 eV. The energy barriers are denoted as L and W , respectively. The sizable difference in the energy barrier for diffusion along the trench and across the dimer reconstruction demonstrates that the diffusion of Cs on GaAs(110) is anisotropic, which might be responsible for the experimentally observed formation of 1D structure as discussed below.

The jump frequency Γ for the surface diffusion of an isolated Cs atom between adjacent equilibrium positions follows an Arrhenius behavior,

$$\Gamma = \nu \exp\left(-\frac{\Delta E_a}{k_B T}\right), \quad (3)$$

where the prefactor of the jump frequency is approximated as $\nu \approx 10^{13}$ Hz for a GaAs surface [15] and ΔE_a is the barrier the Cs atom needs to overcome during the jump.

At room temperature, for the (110) surface the barriers of $\Delta E_a = 0.15$ eV along the [00 $\bar{1}$] direction and of $\Delta E_a = 0.35$ eV along the perpendicular [1 $\bar{1}$ 0] direction result in jump frequencies of $\Gamma = 3 \times 10^{10}$ Hz and 1×10^7 Hz, respectively. This corresponds to an isolated Cs atom diffusing a root-mean-square (rms) distance of $\approx 100 \mu\text{m}$ and $\approx 2.5 \mu\text{m}$ per

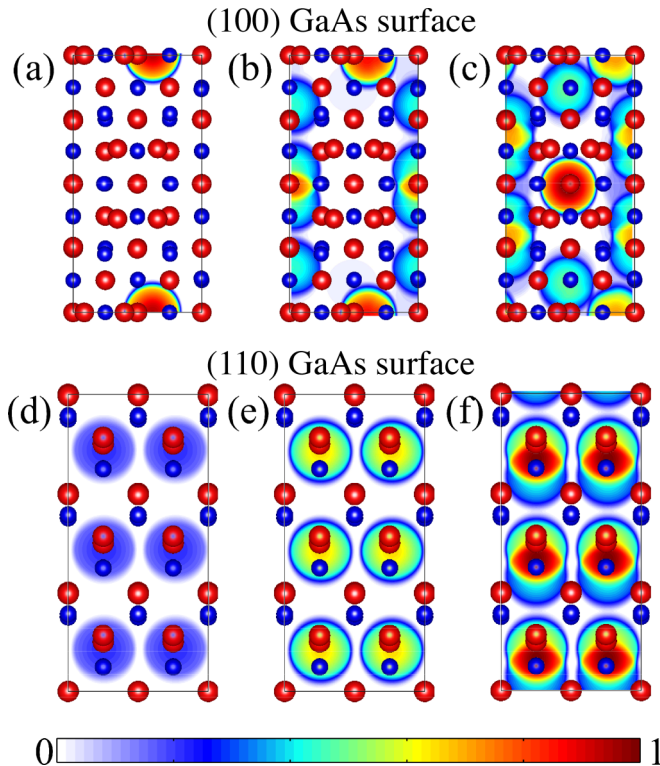


FIG. 3. (Color online) Top view of the Cs position distributions on the (100) surface for Cs surface densities of (a) 0.78, (b) 2.35, and (c) 3.91 atoms/nm², respectively. Top view of Cs position distributions on the (110) surface for Cs densities of (d) 0.74, (e) 2.21, and (f) 3.69 atoms/nm², respectively. The Cs position distributions are overlaid on the surface atoms of the GaAs slabs. The blue circles represent the As atoms and the red circles the Ga atoms. The intensity of the position distribution is indicated by the color bar. The position distributions on the (100) and (110) surfaces are normalized to the maximum of the distribution on that surface over all the Cs densities.

second along the two perpendicular directions, respectively. The 40-times-larger rms displacement of Cs along the [00 $\bar{1}$] direction compared to the [1 $\bar{1}$ 0] direction is likely the reason Cs atoms arrange into 1D line structures at very low Cs surface densities and 2D structures at higher Cs densities, as observed experimentally in STM studies [10,11].

In contrast, on the (100) surface, at room temperature, the large energy barrier of $\Delta E_a = 0.96$ eV along the [01 $\bar{1}$] direction to cross the dimer reconstruction results in $\Gamma = 5 \times 10^{-4}$ Hz, making the Cs atom practically immobile in this direction. The barrier along the trench ([011] direction) is lower with $\Delta E_a = 0.28$ eV, resulting in $\Gamma = 2 \times 10^8$ Hz. The Cs atom can be mobile in this direction and can form 1D chains. However, cluttering of Cs atoms on the (100) results in a severely modified surface potential, as seen from Figs. 3(a)–3(c). This may cause the Cs to become immobile in both directions, resulting in the amorphous growth of Cs on the surface as observed experimentally [13].

It is interesting to note that at temperature of 77 K $\Gamma = 1 \times 10^{-10}$ Hz for $\Delta E_a = 0.35$ eV, making the Cs atom immobile on the (110) surface too. Thus at low temperatures, an amorphous growth of Cs layer might happen on the (110) surface too.

B. Cs position distribution

Figure 3 shows the Cs position distributions as a function of Cs surface densities for the (100) and (110) surfaces. The Cs surface distribution on the (100) surface shows an interesting dependence on surface density. As shown in Fig. 3(a), for low Cs coverages, the Cs atoms stay away from the raised dimer reconstruction and are preferentially located in the trenches. As the Cs density increases in Fig. 3(b), Cs starts to prefer the areas around the dimer and for the highest density studied, Cs atoms preferentially sit atop the dimer reconstruction, as shown in Fig. 3(c). Electron energy loss spectroscopy (EELS) shows the appearance of peaks characteristic to plasmonic oscillations in 2D metallic islands at a Cs coverage of about 0.5 ML [19]. The appearance of these peaks has been interpreted as a phase transformation of the Cs layer in which isolated Cs atoms form 2D clusters on the GaAs(100) surface. This change observed in the EELS spectra and the phase transformation could be caused by the changes in the distribution of the Cs surface positions.

For the (110) surface, Figs. 3(d)–3(f) show that the Cs atoms essentially prefer to stay inside or near the center of the rectangle formed by the surface As atoms at all surface densities. As the Cs density increases, the interactions between the Cs atoms simply broadens the position distribution [Fig. 3(f)].

C. Work-function change and adsorption energy

Figure 4(a) shows that the predicted work-function reduction as a function of Cs surface density agrees well with the experimental results for both GaAs surfaces. The work-function reduction is caused by the change in surface dipole due to charge transfer from the Cs ad-atoms to the GaAs substrate. The work-function reduction (ΔW) is proportional to the change in the surface dipole per unit area (Δp) and is given by $\Delta W = \frac{e}{\epsilon_0} \Delta p$, where e is the electron charge and ϵ_0 the vacuum permittivity. At very low coverages the surface Cs dipoles do not interact and the work function reduces with increasing Cs coverage. However, at higher Cs densities the work function goes through a minimum and then increases due to the interaction between the Cs atoms [21], finally reaching the work function of bulk Cs at very high Cs densities. The simulation shows a slight increase in the work function at Cs surface densities close to 4 atoms/nm² but is still much smaller than the calculated work function of bulk Cs of 1.99 eV. Simulations at higher Cs densities would be needed to confirm the expected rise in work function. Work function at higher Cs surface densities, close to 4 atoms/nm², show a variation of about 100 meV. This work-function variation on the surface could lead to the observed high values of MTE [5].

Figure 4(b) shows how the chemical potential of Cs varies with the Cs surface density for the (100) surface. We see that the agreement between the experimental results and the DFT calculations is quite good for the (100) surface. The continuous reduction in the Cs chemical potential suggests a homogeneous coverage of Cs on the surface.

Figure 4(c) shows the dependence of the Cs chemical potential on the surface density for the (110) surface. The DFT calculations predict a nonmonotonic behavior, suggesting a possible phase separation of the Cs on the surface and that

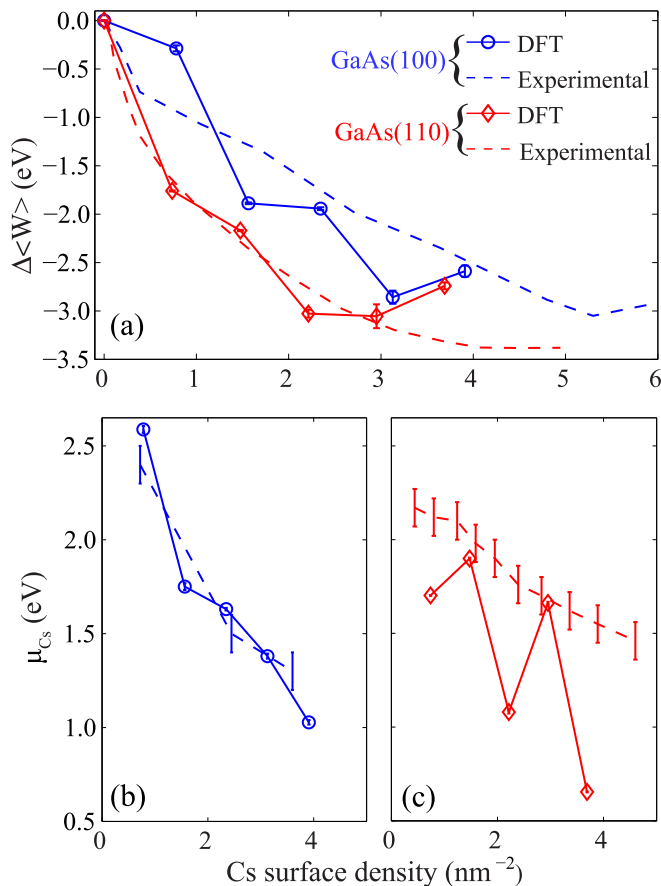


FIG. 4. (Color online) (a) Work-function reduction ($\Delta\langle W \rangle$) as a function of Cs surface density for the GaAs(100) and the GaAs(110) surfaces. The experimental values [13,15] agree well with those calculated using DFT. Chemical potential of adsorbed Cs as a function of Cs surface density for (b) the GaAs(100) and (c) the GaAs(110) surfaces. The experimental values [16,17] are also presented.

Cs atoms could preferentially form clusters. Such clustering is indeed observed on the (110) surface using STM in the form of 1D and 2D Cs structures [10,11]. As the chemical potential is the energy released by adding a Cs atom to the surface, a higher chemical potential corresponds to a lower energy structure of Cs on the surface. Hence, the experimentally observed 1D and 2D structures have lower energy than a uniform Cs coverage, causing the discrepancy in the observed and calculated adsorption energies in Fig. 4(c). Simulating

these structures is beyond the scope of the DFT modeling due to the large size of the required simulation cell. The periodic boundary conditions add constraints due to which formation of lower energy structures is not possible for certain Cs coverages. For these coverages the chemical potential has a lower value than the experimental observations, causing spikes in Fig. 4(c). This behavior is thus an artifact of the constraints enforced by a small simulation cell and periodic boundary conditions.

IV. CONCLUSIONS

Using density functional calculations, we show that the formation of different surface structures observed in the Cs adsorption on the (110) and the (100) surfaces of GaAs can be attributed to the difference in the mobility of Cs atom on these two surfaces. At room temperature, Cs is very mobile on the (110) surface. This allows the formation of low-energy ordered 1D and 2D structures at low coverage and at higher coverage the growth of ordered epitaxial layers on the (110) surface. On the (100) surface at low coverages, Cs atoms are much less mobile, causing them to deposit in an amorphous fashion. Thermodynamic averages of the DFT energies accurately predict the Cs adsorption energy and the work-function reduction of the GaAs surface as a function of Cs coverage. The computational expense currently limits this approach to defect-free surfaces. However, the good agreement of the results with experimental data indicates that defects do not have a strong affect on the adsorption energy and work function.

This work shows that it is possible to computationally screen materials for surface structures and compositions that effectively lower the work function. The computational approach is general and applicable to study the work function for the adsorption of other alkali metals such as Li, Na, and K on various III-V semiconductor surfaces.

ACKNOWLEDGMENTS

This work is supported by the National Science Foundation under Awards No. DMR-0807731 and No. DMR-1056587, through the Cornell Center for Materials Research under Award No. DMR-1120296, and by the Department of Energy under Award No. DE-SC0003965. The research used computational resources of the Texas Advanced Computing Center under Contract No. TG-DMR050028N. The two lead authors, Siddharth Karkare and Laurent Boulet, contributed equally to this work.

- [1] D. T. Pierce, R. J. Celotta, G. C. Wang, W. N. Unertl, A. Galejs, C. E. Kuyatt, and S. R. Mielczarek, *Rev. Sci. Instrum.* **51**, 478 (1980).
- [2] B. Dunham, J. Barley, A. Bartnik, I. Bazarov, L. Cultrera, J. Dobbins, G. Hoffstaetter, B. Johnson, R. Kaplan, and S. Karkare, *Appl. Phys. Lett.* **102**, 034105 (2013).
- [3] D. J. Bradley, M. B. Allenson, and B. R. Holeman, *J. Phys. D: Appl. Phys.* **10**, 111 (1977).
- [4] I. V. Bazarov, B. M. Dunham, Y. Li, X. Liu, D. G. Ouzounov, C. K. Sinclair, F. Hannon, and T. Miyajima, *J. Appl. Phys.* **103**, 054901 (2008).
- [5] S. Karkare, D. Dimitrov, W. Schaff, L. Cultrera, A. Bartnik, X. Liu, E. Sawyer, T. Esposito, and I. Bazarov, *J. Appl. Phys.* **113**, 104904 (2013).
- [6] S. Karkare and I. Bazarov, *Appl. Phys. Lett.* **98**, 094104 (2011).
- [7] S. Karkare, L. Boulet, L. Cultrera, B. Dunham, X. Liu, W. Schaff, and I. Bazarov, *Phys. Rev. Lett.* **112**, 097601 (2014).
- [8] A. J. Van Bommel and J. E. Crombeen, *Surf. Sci.* **45**, 308 (1974).
- [9] A. J. Van Bommel and J. E. Crombeen, *Surf. Sci.* **57**, 109 (1976).
- [10] L. J. Whitman, Joseph A. Stroschio, R. A. Dragoset, and R. J. Celotta, *Phys. Rev. Lett.* **66**, 1338 (1991).

- [11] T. Yamada, J. Fujii, and T. Mizoguchi, *Surf. Sci.* **479**, 33 (2001).
- [12] A. J. Van Bommel, J. E. Crombeen, and T. G. J. Van Oirschot, *Surf. Sci.* **72**, 95 (1978).
- [13] J. Kim, M. C. Gallagher, and R. F. Willis, *Appl. Surf. Sci.* **67**, 286 (1993).
- [14] B. Goldstein, *Surf. Sci.* **47**, 143 (1975).
- [15] J. Derrien and F. A. D'avitaya, *Surf. Sci.* **65**, 668 (1977).
- [16] J. Derrien and F. A. D'avitaya, *Rev. Phys. Appl.* **11**, 377 (1976).
- [17] B. Goldstein and D. Szostak, *Appl. Phys. Lett.* **26**, 111 (1975).
- [18] D. Rodway, *Surf. Sci.* **147**, 103 (1984).
- [19] V. L. Alperovich, O. E. Tereshchenko, A. N. Litvinov, and A. S. Terekhov, *Appl. Surf. Sci.* **175**, 175 (2001).
- [20] L. Giordano, F. Cinquini, and G. Pacchioni, *Phys. Rev. B* **73**, 045414 (2006).
- [21] S. H. Chou, J. Voss, I. Bargatin, A. Vojvodic, R. T. Howe, and F. Abild-Pedersen, *J. Phys.: Condens. Matter* **24**, 445007 (2012).
- [22] A. K. Singh, H. L. Zhuang, and R. G. Hennig, *Phys. Rev. B* **89**, 245431 (2014).
- [23] S. E. Kulkova, S. V. Eremeeva, A. V. Postnikov, and I. R. Shein, *J. Exp. Theor. Phys.* **104**, 590 (2007).
- [24] C. Hogan, D. Paget, Y. Garreau, M. Sauvage, G. Onida, L. Reining, P. Chiaradia, and V. Corradini, *Phys. Rev. B* **68**, 205313 (2003).
- [25] G. Kresse and J. Furthmuller, *Phys. Rev. B* **54**, 11169 (1996).
- [26] P. E. Blochl, *Phys. Rev. B* **50**, 17953 (1994).
- [27] G. Kresse and D. Joubert, *Phys. Rev. B* **59**, 1758 (1999).
- [28] J. P. Perdew, A. Ruzsinszky, J. Tao, V. N. Staroverov, G. E. Scuseria, and G. I. Csonka, *J. Chem. Phys.* **123**, 062201 (2005).
- [29] G. P. Srivastava and S. J. Jenkins, *Phys. Rev. B* **53**, 12589 (1996).
- [30] S. E. Kulkova, D. V. Khanin, and A. V. Subashiev, *Nucl. Instrum. Methods Phys. Res., Sect. A* **536**, 295 (2005).
- [31] G. Mills, H. Jonsson, and G. K. Schenter, *Surf. Sci.* **324**, 305 (1995).
- [32] H. Jonsson, G. Mills, and K. W. Jacobsen, in *Classical and Quantum Dynamics in Condensed Phase Simulations*, edited by B. J. Berne, G. Cicciotti, and D. F. Coker (World Scientific, Singapore, 1998).